THE ROLES OF STRENGTH ON SHOCK-INDUCED DEVOLATILIZATION FROM CALCITE. K. Kurosawa[1], H. Genda[2], S. Azuma[3] and K. Okazaki[4], [1]Planetary Exploration Research Center, Chiba Institute of Technology (2-17-1, Tsudanuma, Narashino, Chiba 275-0016, Japan, ¥osuke.kurosawa@perc.it-chiba.ac.jp), [2]Earth-Life Science Institute, Tokyo Institute of Technology, [3]Department of Earth & Planetary Sciences, Tokyo Institute of Technology, [4]Kochi Institute for Core Sample Research, JAMSTEC.

Introduction: Mutual collisions between two small bodies at the main belt region at velocities higher than several km s^{-1} cause heating of their surface materials [e.g., 1]. This impact heating results in a variety of thermal metamorphism [e.g., 2], including the devolatilization from volatile-bearing minerals, the change in optical properties, the reset of ^{40}Ar-^{39}Ar age, and melting. It has been widely accepted that the degree of impact heating depends strongly on the impact velocity [e.g., 1]. Given that we have an accurate understanding of the relation between the degree of thermal metamorphism and impact condition, analyses of thermally-metamorphosed meteorites allow us to decode the impact environment in the solar system through its history [e.g., 3].

Recently, Kurosawa and Genda (2018) [4] reported that plastic deformation of the shock-comminuted rocks efficiently converts the kinetic energy in the impact-driven flow field into the internal one, resulting in a much higher degree of impact heating than previously expected. This heat source has been overlooked for a long time [5]. This new finding was obtained based on the iSALE-Dellen [e.g., 6-9], which can treat elasto-plastic behavior of rocky materials. If a temperature rise due to plastic deformation is also significant in natural impact phenomena, impact histories derived from thermal metamorphism would need to be revised [4, 10].

Here, we examine the validity of the computed results by comparing the experimental data on shock-induced devolatilization from natural calcite samples. Kurosawa et al. (2012) measured the shock-generated CO_2 mass $M_{CO2,exp}$ in an open system at impact velocities ranged from 2 to 7 km/s [11]. In this study, we simulate seven impacts performed by [11] by using the iSALE-2D combined with a constitutive model, and estimate the CO_2 production in the computations $M_{CO2,calc}$ based on thermodynamic calculations.

Calculation setting: The "ROCK" model in the iSALE package [e.g., 9, 12] was used to treat elasto-plastic behavior of calcite targets. The model is a combination between the Lundborg [13] and the Drucker-Prager models [14] for intact and damaged rocks, respectively. The two models are combined via a damage parameter, which is determined by total plastic strain [e.g., 7]. The parameter set for limestone [15] was used for calcite targets. To explore the role of material strength on the degree of impact heating,

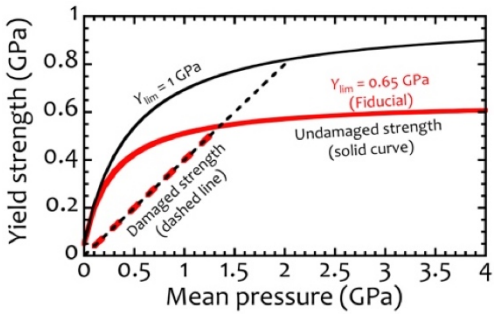

Figure 1. The strength model used in this study.

we varied the von-Mises limit Y_{lim} as a free parameter. The fiducial value of Y_{lim} determined by [15] is Y_{lim} = 0.65 GPa. We also used the thermal softening model by [16] to treat the effects of strength lowering with increasing temperature. Figure 1 shows the yield strength as a function of temporal pressure in a medium. We made a variety of stress curves by changing Y_{lim} as shown in the figure.

The impact velocities v_{imp} in the simulation were set to the same values achieved in the impact experiments [11]. The ANEOS [17] for calcite [18, 19] and the Tillotson EOS [20] with the parameters for Al_2O_3 were used for targets and projectiles, respectively. An Al_2O_3 projectile with the diameter D_p of 3.2 mm was divided into 200 cells per projectile radius (CPPR). A calcite target was set as a cylinder with 2,000 cells per target radius. Lagrangian tracer particles are inserted into each cell. We stored temporal pressure P and entropy S into each tracer. Since [11] used non-porous polycrystalline natural calcite samples, we did not include any porosity compaction models.

CO_2 production in iSALE: We calculated the degree of devolatilization ψ of each tracer particle by the lever rule. The entropies of incipient and complete devolatilization of calcite S_{id} and S_{cd} are given by [11]. The CO_2 production M_{CO2} was estimated to be $M_{CO2} = \Sigma(\psi_i \Delta m_i)$, where subscript i indicates the tracer ID and Δm is the mass of tracer particle. Since S gradually increases during decompression until pressure decreases down to ~1 GPa in the case with the material strength, we used the S value at 1 GPa stored on each tracer that is once shocked (>3 GPa) but is released down to <1 GPa to calculate M_{CO2} at each time step. When v_{imp} is sufficiently high, we confirmed that M_{CO2} gradually increases with time, and become a

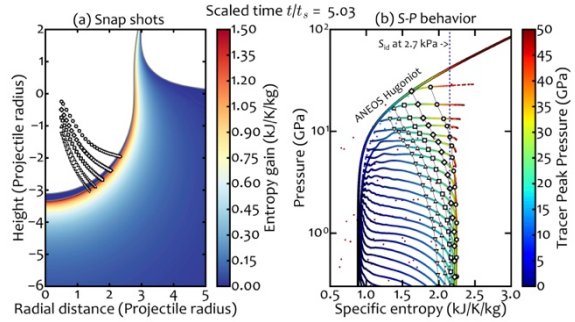

Figure. 2. (a) Snap shot at t = 5 t_s, v_{imp} = 4.14 km/s and Y_{lim} = 0.65 GPa. The color map means the entropy gain. (b) The thermodynamic track on a entropy-pressure plane. The color indicates the peak pressures of tracer particles.

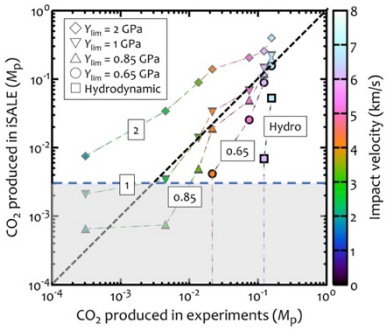

Figure 3. $M_{CO2,exp}$ vs $M_{CO2,calc}$. The color bar indicates impact velocity.

nearly constant by t = 5 t_s, where $t_s = D_p/v_{imp}$. Consequently, we employed the M_{CO2} at t = 5 t_s as $M_{CO2,calc}$ and used to compare with $M_{CO2,exp}$.

Results: Figure 2a shows a snap shot of the calculation along with the trajectories of five selected tracers initially located at r = 0.76 R_p, where r is radial distance from the symmetry axis. The highly-heated calcites are concentrated into near the crater wall. Figure 2b shows the thermodynamic tracks on a *S*-*P* plane of the tracers initially located at the same radial distance of the five selected tracers. The result shows that the condition where $S > S_{id}$ is achieved even at the peak pressure of 25 GPa, which is much lower than the required peak pressure for incipient devolatilization (47 GPa) estimated by [11].

Figure 3 shows $M_{CO2,exp}$ vs $M_{CO2,calc}$. If the data point is plotted on the straight line inclined 45 degrees on this diagram, $M_{CO2,calc}$ coincides with $M_{CO2,exp}$. We conducted total 35 runs with 4 different Y_{lim} values and without material strength (i.e., purely hydrodynamic). The grey hatched region means non-reliable due to the low spatial resolution. We found that $M_{CO2,calc}$ in the hydrodynamic and the fiducial case is systematically lower than $M_{CO2,exp}$. In contrast, $M_{CO2,calc}$ becomes systematically larger than $M_{CO2,exp}$ when we used Y_{lim} = 2 GPa. With Y_{lim} = 1 GPa, $M_{CO2,calc}$ values are close to $M_{CO2,exp}$.

Discussion & Conclusions: The similarity between $M_{CO2,exp}$ and $M_{CO2,calc}$ at Y_{lim} = 1 GPa suggests that the iSALE computation could reproduce the thermodynamic response of shocked natural calcite samples although we should use a slightly larger Y_{lim} (1 GPa) value compared to the fiducial value (0.65 GPa). The difference may be explained by the dynamic failure mechanism [e.g., 21] as pointed out by [5]. Although the strength model employed in this study is constructed based on static failure data, the brittle solids become stronger at a higher strain rate. The strain rate in hypervelocity impact experiments (~10^6 s^{-1}) is much higher than that usually achieved in static failure experiments (<10^{-4} s^{-1} [e.g., 22]). The thermal softening due to impact heating, however, has the opposite effect. Based on above discussion, we proposed that "effective" Y_{lim} for calcite, including the effects of the differences in strain rate and in temperature, is approximated as 1 GPa. Our results enhance the significance of the recent finding on impact heating by [4].

Acknowledgements: We appreciate the developers of iSALE, including G. Collins, K. Wünnemann, B. Ivanov, J. Melosh, and D. Elbeshausen. We also thank Tom Davison for the development of the pySALEPlot.

References: [1] Ahrens, T. J. & O'Keefe, J. D. (1972), *The Moon*, **4**, 214-249. [2] Stöffler, D. et al. (1991), *MaPS, 3,* 5-49. [3] Marchi S. et al. (2013) *Nature Geoscience*, **6**, 303-307. [4] Kurosawa, K. & Genda H. (2018), *GRL*, **45**, 620-626. [5] Melosh, H. J. & Ivanov, B. A. (2018), *GRL*, **45**, 2597-2599. [6] Amsden A. A., et al. (1980) *LANL Report* LA-8095. 101 p. [7] Ivanov B. A., et al. (1997), *IJIE*, 20, 411. [8] Wünnemann, K., et al. (2006), *Icarus*, 180, 514. [9] Collins, G. S. et al. (2016), *Figshare*, 10, m9. https://doi.org/10.6084/m9.figshare.3473690.v2. [10] Wakita, S. et al. (2019), *GRL*, **46**, 13678-13686. [11] Kurosawa K. et al. (2012) *EPSL*, **68,** 337-338. [12] Collins G. S. et al. (2004), *MaPS*, **39**, 217-231. [13] Lundborg, N. (1968), *Int. J. Rock Mech. Min. Sci.*, **5**, 427-454. [14] Drucker, D. C. & Prager, W. (1952) *Quarterly of Applied Mathematics*, **10**, 157-165. [15] Goldin, T. J. et al. (2006) *MaPS*, **41**, 1947-1958. [16] Ohnaka, M. (1995), *GRL*, **22**, 25-28. [17] Thompson, S. & Lauson, H. (1972), *SNL Report*, SC-RR-71 0714:113p.[18] Pierazzo, E. et al. (1998), *JGR*, **103**, 28,607-28,625. [19] Ivanov, B. A. (2019), *Private comm.* [20] Tillotson, J. H. (1962). *Technical Report GA-3216*, General Atomic Report. [21] Ramesh, K. T. et al. (2015) *P&SS*, **107**, 10-23. [22] Hacker, B. R. & Kirby, S. H. (1993), *Journal of Structural Geology*, **15**, 1207-1222.